Journal of Science and Technology in Civil Engineering, HUCE, 2026, 20 (4): 81–96

A COMPARATIVE STUDY OF DAMAGE IDENTIFICATION OF A STEEL BRIDGE GIRDER USING NUMERICAL MODAL ANALYSIS

Piseth Doung[a,b,*], Sereyvathanak Lun[c]

[a]*Department of Civil Engineering, Faculty of Civil Engineering, Institute of Technology of Cambodia, PO Box 86, Russian Fed. Blvd., Phnom Penh, Cambodia*
[b]*Research and Innovation Center, Institute of Technology of Cambodia, PO Box 86, Russian Fed. Blvd., Phnom Penh, Cambodia*
[c]*Department of Transport and Infrastructure Engineering, Faculty of Civil Engineering, Institute of Technology of Cambodia, PO Box 86, Russian Conf. Blvd, Phnom Penh, Cambodia*

Article history:
Received 06/2/2026, Revised 26/8/2026, Accepted 28/8/2026, Available online 16/10/2026, Version of Record 25/12/2026

Abstract

A steel bridge girder is one of the crucial structural components in transportation infrastructure. It is typically exposed to corrosion over time, leading to a reduction in steel thickness and deterioration of structural performance. Early detection and localization of such damage are essential for ensuring structural safety and longevity. This study presents a comparative numerical investigation on vibration-based damage identification for a steel bridge girder using modal analysis. The purpose is to identify damage in a steel girder, considering the effects of damage size and location, meshing, and element type in the numerical simulation. A simply-supported steel girder with a span length of 15.2 m was selected for the analysis using both beam and solid element models in Abaqus/CAE. Damage was modeled as an equivalent reduction in Young's modulus to represent the stiffness loss associated with corrosion or cracking, rather than explicitly simulating geometric section loss. The reduction in Young's modulus was introduced at the support, 1/4-span, and 1/2-span, while the influence of mesh density and element type was also investigated. Three damage indices, namely Modal Curvature Damage Index (MCDI), Modal Strain Energy Damage Index (MSEDI), and Modal Flexibility Damage Index (MFDI), were then evaluated and compared. The results showed that damage at 1/2-span produced the most significant reduction in natural frequencies, while multiple damages showed cumulative effects. For MCDI and MSEDI, Modes 1 and 3 offered reliable damage localization, whereas other modes demonstrated complexity due to multiple curvature effects. MFDI provided more effective damage localization when all mode shapes and natural frequencies were considered. Mesh density affected damage quantification but not localization. Damage quantification varied between three damage indices for different mesh densities. It was also found that beam elements were computationally efficient, while solid elements provided greater flexibility for representing localized stiffness changes. This study provided a simple and practical guidance for the Structural Health Monitoring modeling of steel bridge girders. However, it should be noted that this study is limited to Young's modulus reduction as an equivalent local stiffness loss. To better capture the damage, actual geometry modeling of corrosion or cracking should be further studied.

Keywords: damage identification; finite element; modal analysis; steel bridge girder; structural health monitoring (SHM).

1. Introduction

Steel bridge girders play a crucial role in supporting and sustaining the structural integrity of a bridge, especially when a bridge is subjected to heavy traffic and dynamic loads, as illustrated in

*Corresponding author. *E-mail address:* piseth@itc.edu.kh (Doung, P.)
https://doi.org/10.31814/stce.huce2026-20(4)-06 p-ISSN 1859-2996; e-ISSN 2734-9268
© 2026 The Author(s). Published by Hanoi University of Civil Engineering. Licensed under CC BY-NC-ND 4.0.

Fig. 1. A steel bridge girder is usually subjected to extreme conditions such as fatigue [1], overload [2], corrosion [3], and collision [4]. Under severe atmospheric conditions, the steel girders always face a challenge against corrosion, especially in the lower part of the girder. That is because the lower parts are potentially subjected to liquid disposal and other harsh environmental conditions. When a steel girder is locally damaged, the material condition deteriorates, and the thickness of structural members decreases, which has a direct impact on its stiffness. As stiffness decreases, the structure's modal properties, such as natural frequencies and mode shapes, noticeably change. If correctly identified and interpreted, these variations can serve as important indicators of damage identification. Damage identification-based numerical modal analysis provides rigorous potential, but its successful implementation is dependent on critical methodological choices. It has to find a balance between numerical modeling precision, such as comparison of beam elements versus solid elements, and the performance of damage identification techniques. However, the performance of damage identification techniques is also affected by the level of mesh sizes used in the simulation. The capture of localized damage effects, which is important for these identification methods, is significantly impacted by both element type and mesh size. The set of mode shapes chosen for analysis has a significant impact on the sensitivity and accuracy of these methods. This problem has been addressed in this study to identify the damage of the steel bridge girder using numerical modal analysis.

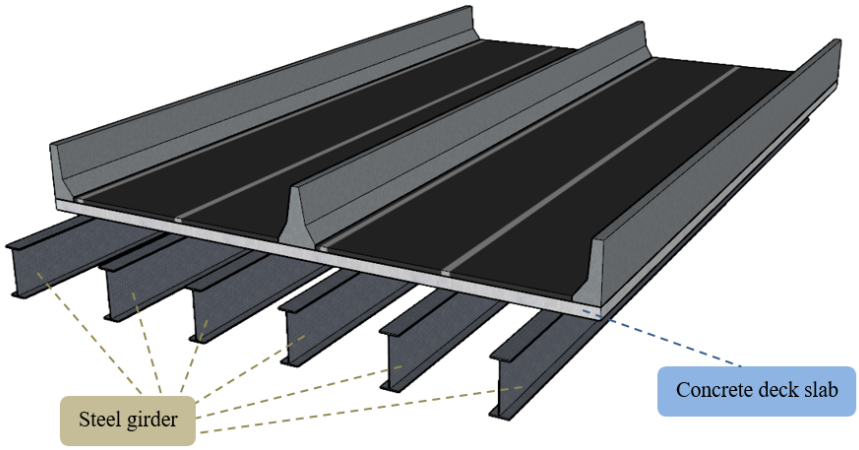


Figure 1. Steel bridge girder components

Traditionally, bridge conditions were assessed primarily through visual inspection. Only visible damage can be detected using this non-destructive evaluation method. Structural Health Monitoring (SHM) refers to a non-destructive structural evaluation process of tracking and assessing the safety and performance of the structure using an on-structure sensing system [5, 6]. SHM is defined as the process of implementing an automated and online damage detection strategy in a structure [7, 8]. SHM has traditionally been carried out using two main approaches: model-based and data-based methods [9]. However, in recent years, a hybrid approach to SHM has emerged, combining principles from both model-based and data-based approaches [10] to enhance the accuracy and robustness. The model-based approach is divided into two stages, including undamaged and damaged stages, as shown in Fig. 2. Each stage involves the calibration of numerical finite element (FE) models. During the first stage, an initial FE model is calibrated using data from the undamaged condition to create a validated FE model or reference model. In the second stage, the reference model is calibrated using data from the damaged condition (after the operational and environmental conditions have been eliminated). Damage identification is then performed based on variation in extracted parameters between

undamaged and damaged stages [11].

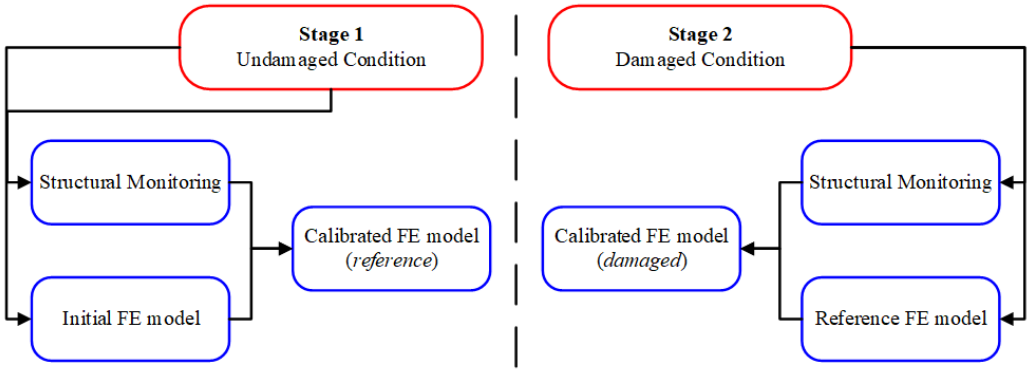


Figure 2. The model-based SHM approach [11]

Damage identification in a structural system is the process of examining changes in measured responses to detect, locate, and characterize damage [12]. Rytter [13] proposed four levels in the damage identification process and a damage prognosis level, as shown in Fig. 3, such as damage detection (Level 1), damage localization (Level 2), damage quantification (Level 3), and remaining life prediction (Level 4).

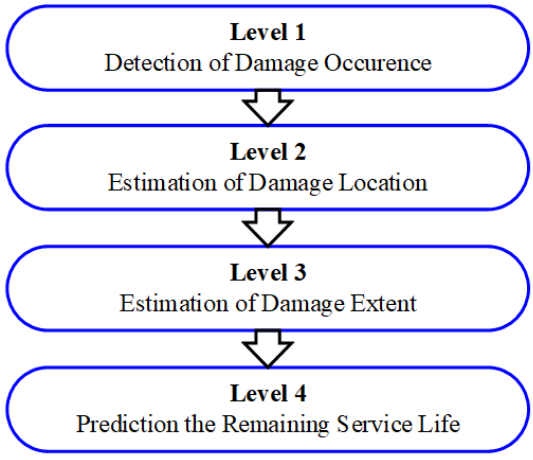


Figure 3. Schematic diagram of damage identification [13]

Among the existing damage identification methods, vibration-based damage identification methods have gained significance in recent decades due to their non-destructive and monitoring techniques capable of identifying damage using changes in dynamic characteristics [14]. The fundamental principle behind vibration-based damage identification techniques is that damage affects the structure's dynamic properties, such as natural frequencies, mode shapes, and modal damping [15, 16]. The changes in vibration parameters can be used as a damage indicator for damage identification. These methods use features extracted from dynamic parameters and are classified as mode shape-based, natural frequency-based, and other modal parameter-based methods [17, 18].

This study presents a comparative case study on damage identification of a simply-supported steel girder using numerical modal analysis in terms of damage indices. A W30x116 steel girder with a span of 15.2 meters was modeled using the beam and solid elements in Abaqus/CAE. Damage

scenarios were simulated through reductions in Young's modulus of 25%, 50%, and 75% at three key locations (support, 1/4-span, and 1/2-span), with varying mesh densities. The study evaluated three modal-based damage indices, namely Modal Curvature Damage Index (MCDI), Modal Strain Energy Damage Index (MSEDI), and Modal Flexibility Damage Index (MFDI). The results of the parametric sensitivity on damage identification were analyzed and discussed in the following sections.

2. Theoretical review

2.1. Fundamentals of modal analysis

In general, modal analysis is carried out for estimating the modal parameters such as natural frequencies, damping, and mode shapes of a structure. The modal parameters will depend on geometry, material properties, and boundary conditions, which can be extracted by implementing operational modal analysis (OMA) or experimental modal analysis (EMA) [19].

The dynamic behavior of a structure can be expressed by Eq. (1) as:

$$[M]\{\ddot{u}(t)\} + [C]\{\dot{u}(t)\} + [K]\{u(t)\} = \{F(t)\} \tag{1}$$

where $[M]$ is the mass matrix, $[C]$ is the damping matrix, $[K]$ is the stiffness matrix, $\{u(t)\}$, $\{\dot{u}(t)\}$, $\{\ddot{u}(t)\}$, and $\{F(t)\}$ are the displacements, velocities, accelerations. And force as functions of time, respectively.

For undamped free vibration ($[C] = 0$, and $\{F(t)\} = 0$), the solution is assumed in a harmonic form:

$$\{u(t)\} = \{\phi\}\, e^{i\omega t} \tag{2}$$

Substituting Eq. (2) into Eq. (1) yields the eigenvalue problem:

$$\Big([K] - \omega^2 [M]\Big)\{\phi\} = 0 \tag{3}$$

where ω is the circular natural frequency, and $\{\phi\}$ is the mode shape vector. Solving this eigenvalue problem involves finding the specific values of ω^2 (the eigenvalues) for which non-trivial solutions for $\{\phi\}$ (the eigenvectors) exist.

2.2. Modal curvature-based damage index (MCDI)

Pandey et al. [20] first proposed modal curvature changes as a damage indicator for localization. MCDI was assessed in both a cantilever and a simply supported beam. Mode shape curvature is related to the bending strain of a beam cross-section, since the curvature at a point is given by Eq. (4).

$$\phi'' = \frac{M}{EI} \tag{4}$$

where ϕ'' is the mode shape curvature, M is the bending moment, E is the elasticity modulus, and I is the moment of inertia. Eq. (5) shows how the central difference approximation is used to compute the curvature mode shapes from the displacement mode shapes.

$$\phi''_{i,j} = \frac{\phi_{i+1,j} - 2\phi_{i,j} + \phi_{i-1,j}}{h^2} \tag{5}$$

where i is the node number, j is the mode shape number, and h is the length between node i to $i + 1$. In this study, the boundary nodes at the start and end also produced inaccurate peaks in the damage indices. Therefore, their curvature values were set to zero to reduce boundary errors and improve damage localization in the interior region. The element that has the greatest absolute difference

between the undamaged and damaged states determines the damage location called modal curvature-based damage index that denoted MCDI:

$$MCDI_{i,j} = \left|\left(\phi''_{i,j}\right)_d - \left(\phi''_{i,j}\right)_u\right| \tag{6}$$

where d and u denote the damaged and undamaged states, respectively.

2.3. Modal strain energy-based damage index (MSEDI)

Stubbs et al. [21] developed the first damage detection method based on a change in modal strain energy. Kim and Stubbs [22, 23] first developed the MSEDI to evaluate the integrity of beam-like structures. Kim and Stubbs [24] also proposed an improved damage identification method based on modal information and evaluated its accuracy on a two-span continuous beam.

The MSEDI method determines changes in strain energy in deformed beams with specific mode shapes. These changes were used to generate a damage index. Eq. (7) will be used to calculate the modal strain energy of a beam.

$$U = \int \frac{EI}{2}\left(\frac{d^2\phi}{dx^2}\right)^2 dx \tag{7}$$

where EI is the flexural stiffness, $\frac{d^2\phi}{dx^2}$ is the mode shape curvature, and x is the distance along the beam length. The damage index MSEDI for the j-th element and i-th mode shapes of the beam is given by Eq. (8) [22, 23].

$$MSEDI_{i,j} = \frac{\left[\left(\phi''_{i,j}\right)_d^2 + \sum\left(\phi''_{i,j}\right)_d^2\right]\left[\sum\left(\phi''_{i,j}\right)_u^2\right]}{\left[\left(\phi''_{i,j}\right)_u^2 + \sum\left(\phi''_{i,j}\right)_u^2\right]\left[\sum\left(\phi''_{i,j}\right)_d^2\right]} \tag{8}$$

2.4. Modal flexibility-based damage index (MFDI)

Pandey and Biswas [25] originally proposed the modal flexibility method, which uses changes in modal flexibility as a damage indicator, to detect damage in beams. Wahalathantri et al. [26] investigated four damage indices based on modal flexibility change in order to compare damage-detection accuracy with a reduced number of data acquisition points. The damage index found to perform best at locating damage is the modal flexibility-based damage index (MFDI). This method incorporates both the natural frequencies and mode shapes of a structure. The modal flexibility, F, of a linear structure can be expressed as in Eq. (9).

$$[F] = \sum_{j=1}^{m}\left[\frac{1}{\omega_j^2}\right]\left[\phi_j\right]\left[\phi_j\right]^T \tag{9}$$

where j is the mode number, m is the total mode number considered, ω_j is the j-th circular natural frequency, $\left[\phi_j\right]$ is the j-th mode shape vector, and $\left[\phi_j\right]^T$ is the j-th mode shape vector transpose.

The damage index found to perform best at locating damage, the modal flexibility-based damage index (MFDI), is given in Eq. (10) [26]. The MFDI is defined as the column-wise maximum of the modal flexibility change matrix.

$$MFDI = \frac{[F]_d - [F]_u}{[F]_u} \tag{10}$$

3. Case study of a steel bridge girder

This case study detailed a numerical investigation on damage detection and localization in a steel bridge girder using numerical modal analysis. The objective is to assess and compare the performance of three modal-based indices (MCDI, MSEDI, and MFDI) considering the parametric sensitivity, such as element types, mesh density, and damage size and location in Abaqus/CAE. Damage was simulated through reductions in Young's modulus at selected locations, and the effects of mesh density and mode shape selection are also evaluated accordingly. Fig. 4 depicts an overall framework used to assess the damage identification in this study.

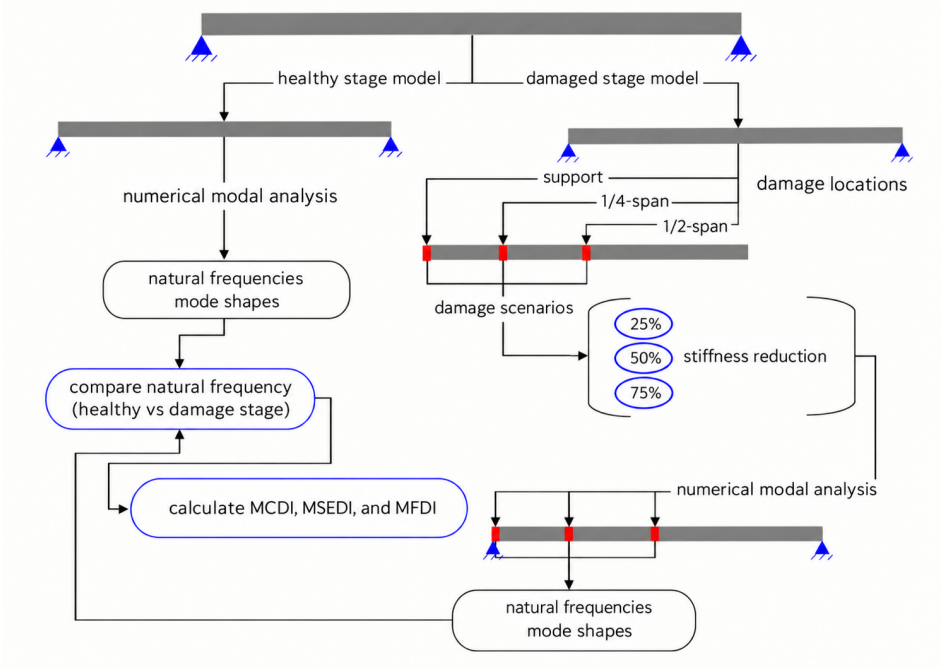


Figure 4. Overall framework for damage identification

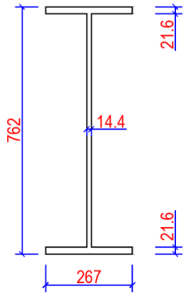
This study was conducted using noise-free data from finite element analysis. In practice, measured mode shapes are affected by noise. Previous studies simulated random white Gaussian noise on the mode shape data. The reported results showed that MCDI and MSEDI were sensitive to noise due to their second-order derivatives, while MFDI remained locating both single and multiple damage locations even under 5% and 10% noise levels [14].

3.1. Description of a steel girder

The case study was conducted using a numerical approach based on a steel bridge girder of the Alamosa Canyon Bridge. [27] The Alamosa Canyon Bridge is located near the town of Truth or Consequences in southern New Mexico and is approximately aligned in the north and south direction was constructed around 1937, as shown in Fig. 5(a). This bridge has seven independent spans. Each span consists of a concrete deck supported by six W30x116 steel beams. The detailed dimensions of the W30x116 section can be seen in Fig. 5(b). The roadway in each span is approximately 7.3 m wide and 15.2 m long. A pinned-pinned boundary condition was proposed in this study.



(a) Alamosa Canyon Bridge



(b) W30x116-section (unit in mm)

Figure 5. View of Alamosa Canyon Bridge and cross-section [27]

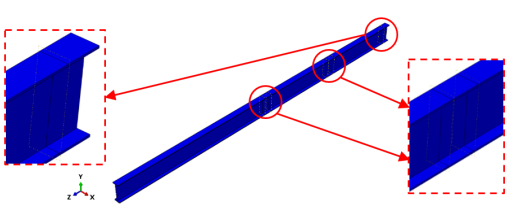
3.2. Finite element modeling

The finite element modeling was performed using Abaqus/CAE, employing two approaches (solid and beam elements). Structural steel was defined using the elastic properties for both elements, as shown in Table 1. Three separate models were meshed by entering specific global seed sizes to achieve different mesh densities: 380 mm seed size, 304 mm seed size, and 253.3 mm seed size. For mesh element types, C3D8R was used for the solid element model and B31 for the beam element model.

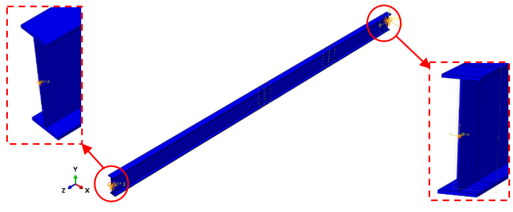
Table 1. Material properties

Description	Value
Young's modulus	200000 MPa
Poisson's ratio	0.3
Density	7.85×10^{-9} ton/mm^3

For the solid element model, the girder was modeled as a 3D solid using an extrusion of a 2D I-section in XY plane representing a W30x116 steel section. The steel girder is oriented along the longitudinal Z-axis with a total length of 15.2 m. To control and localize damage positions, five X-Y datum planes were created at specific distances, such as support, 1/4-span, and 1/2-span. Each damage location was defined using two datum planes, as illustrated in Fig. 6(a). Reference points were created at the centroids of the end cross-sections and coupled to the corresponding support surfaces using coupling. The pinned–pinned boundary conditions were then applied at these reference points, as shown in Fig. 6(b).



(a) Partition at damage location

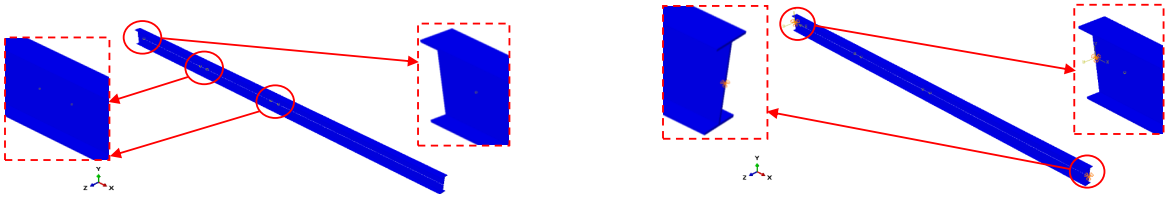


(b) Pinned-pinned support

Figure 6. Partition and boundary condition (solid element)

For the beam element model, the beam geometry was defined as a 3D deformable wire part. Along the global X-axis, a single line segment measuring 15.2 m. To control and localize damage

positions, five datum points were created at specific distances at the support, 1/4-span, and 1/2-span. Each damage location was enclosed by two datum points as shown in Fig. 7(a). Boundary conditions were applied to node sets associated with the respective end faces as shown in Fig. 7(b).

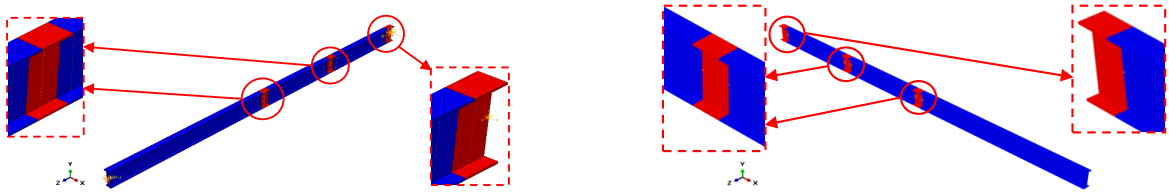


(a) Partition at damage location (b) Pinned-pinned support

Figure 7. Partition and boundary condition (beam element)

3.3. Simulation of damage scenario

Based on the critical stress location due to shear force and bending moment in a bridge girder, three specific locations along the girder span were considered for damage simulation at the support, 1/4-span, and 1/2-span separately, which was called the single damage case. For the multiple damage case, damage was simulated across three locations simultaneously. These locations were chosen due to their vulnerability to shear cracking (near supports), bending fatigue (near mid-span), and combined stress effects (near quarter span), as shown in Fig. 8(a) for the solid element, Fig. 8(b) for the beam element. For each of the three damage locations, three different damage levels were considered, corresponding to reductions in Young's modulus (E) by 25%, 50%, and 75%. These stiffness reductions were applied only to the proposed segments of the models that correspond to the damage. Table 2 describes the damage scenarios applying to the study steel girder.



(a) Partitioned at damage zones (solid model) (b) Partitioned at damage zones (beam model)

Figure 8. Partitioned girder with damage zone

Table 2. Damage scenario

Location	Single damage								
	Support			1/4-span			1/2-span		
Damage case	SD1	SD2	SD3	SD4	SD5	SD6	SD7	SD8	SD9
E-reduction (%)	25%	50%	75%	25%	50%	75%	25%	50%	75%
Location	Multiple damage								
Damage case	MD1			MD2			MD3		
E-reduction (%)	25%			50%			75%		

The damage simulation was implemented by reducing the Young's modulus of the steel material to 150000 MPa, 100000 MPa, and 50000 MPa, representing reductions of 25%, 50%, and 75%,

respectively. These materials were assigned to the partitioned damage regions using the assign section tool in the property module. In this simulation, steel density was not necessarily changed.

To perform damage localization, displacement data for selected mode shapes were extracted manually from Abaqus. For both the solid element and beam element models, a series of nodes along the girder's longitudinal direction was manually selected to represent the vibration shape. The node spacing along the girder span was defined according to the mesh discretization used in the finite element model. The mesh sizes of 380 mm, 304 mm, and 253.3 mm, corresponding to 40, 50, and 60 segments, respectively, were applied to a steel girder with a length of 15.2 m. From each selected node, the displacement values in the nodal displacement were captured for the six mode shapes, and the results were described and discussed in the next section.

4. Results and discussion

4.1. Mode shapes and natural frequencies

Mode shapes are motion patterns that result in all parts of a structure vibrating at a specific natural frequency. Mode shapes are suitable for Level 2 and Level 3 of damage identification as they contain partial structural information [28]. After performing the modal analysis in Abaqus, the first six flexural modes were carried out for both the solid and beam element models. The mode shapes of the undamaged and damaged models were compared through visualization based on their bending direction and deformation patterns. Since the corresponding patterns remained similar and no mode switching was observed, Modes 1 to 6 were directly matched between the undamaged and damaged cases. The displacement component used for extraction was chosen according to the major bending direction of each mode. Five modes demonstrated lateral bending conditions, and therefore, the lateral displacement component was used. In contrast, the vertical displacement component was used in Mode 3, which corresponds to vertical bending conditions. Each mode bent in different curvatures for both horizontal and vertical directions, as shown in Figs. 9 and 10. Since the damage locations predicted by all three mesh sizes were essentially identical, the 253.3 mm mesh may be considered sufficiently fine for the present analysis. Further refinement beyond 253.3 mm did not improve damage localization and instead increased mode shape complexity.

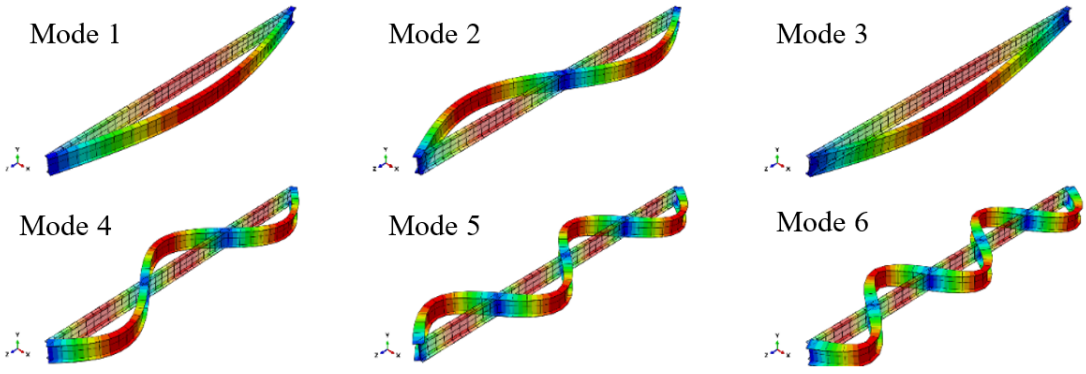


Figure 9. First six bending displacement modes (solid model)

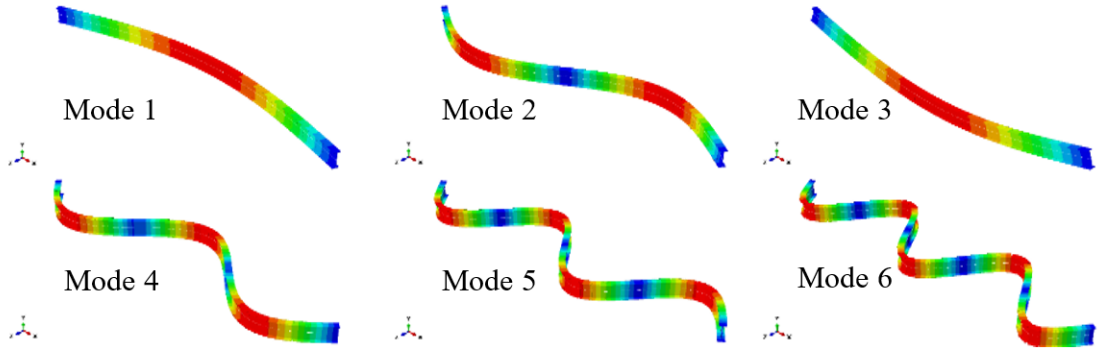
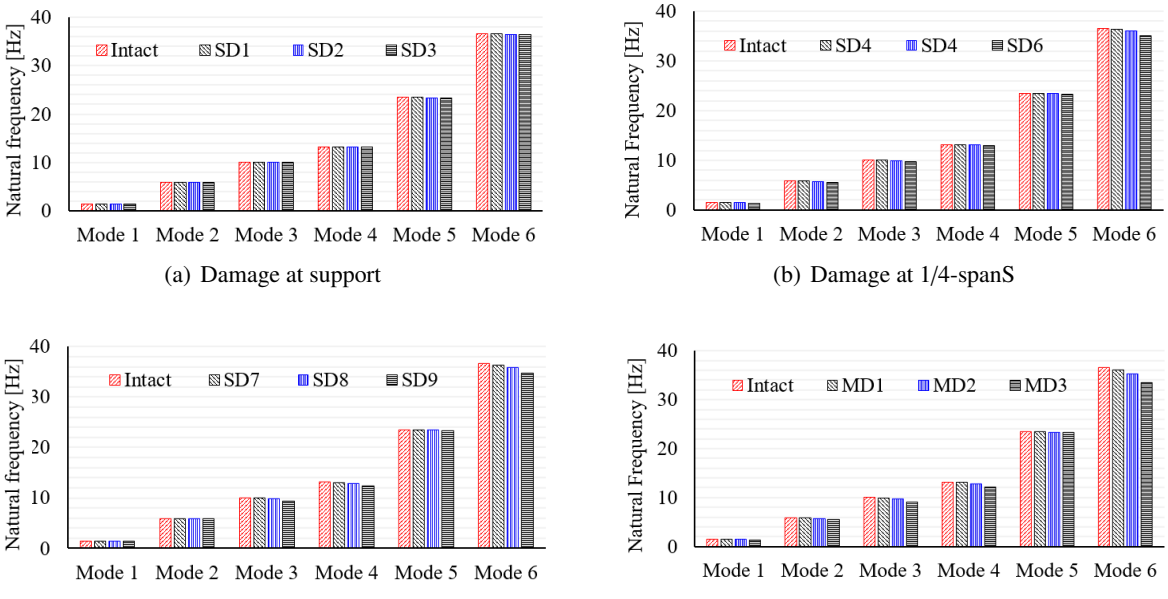


Figure 10. First six bending displacement modes (beam model)

The natural frequencies of the first six modes were compared between the undamaged and damaged models to detect the presence of damage. The results showed that stiffness reduction led to a decrease in natural frequencies. Figs. 11(a) to 11(c) illustrate the variation in natural frequencies of a steel bridge girder modeled under single damage cases. The results indicated very small variations in natural frequency for the first three modes, indicating limited sensitivity to damage located near the support region. In contrast, damage introduced at 1/2-span results in significantly larger reductions in natural frequency for the same levels of stiffness reduction, demonstrating the higher sensitivity of modal parameters to damage at regions of maximum bending. Higher-order modes demonstrated high effectiveness in detecting damage, particularly in the central regions of the girder. Furthermore, as illustrated in Fig. 11(d), MD1, MD2, and MD3 produced greater frequency reductions compared to single damage cases, confirming that cumulative damage led to additional stiffness reduction and significant changes in dynamic behavior.



(a) Damage at support

(b) Damage at 1/4-spanS

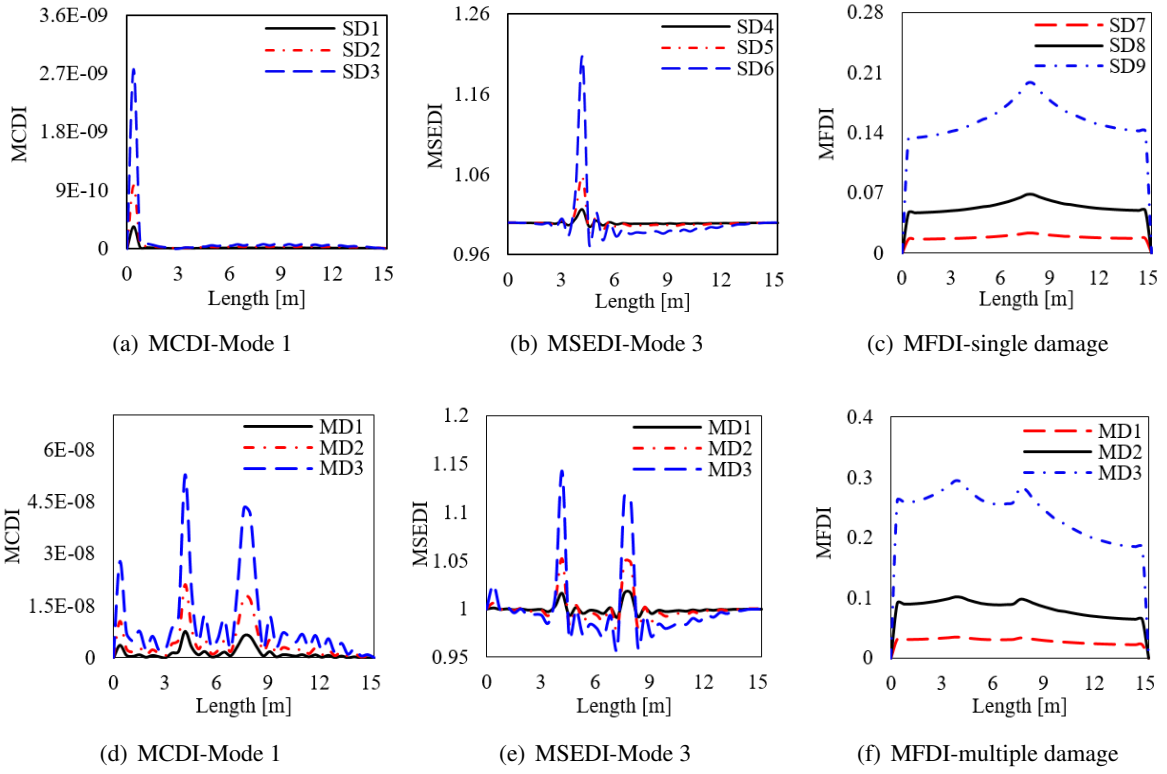
(c) Damage at 1/2-span

(d) Multiple damage

Figure 11. Natural frequency-based damage detection

4.2. Evaluation of damage indices

Both MCDI and MSEDI are effective at localizing single and multiple damage to both beam and solid elements. Figs. 12(a), 12(b), 12(d), and 12(e) illustrate the performance of the MCDI and MSEDI along the girder length for the solid model with a 380 mm mesh. For both damage indices, distinct peaks are observed at the predefined damage locations for single damage and multiple damage cases, while the remainder of the girder demonstrates significantly lower index values. In particular, the peak damage index values at the damaged sections are several times larger than values along undamaged regions, indicating localization capability. The positions of these peaks coincide with the actual damage locations, confirming the accuracy of damage localization. In addition, the peak magnitudes increase with increasing damage severity (25% to 75% stiffness reduction), indicating that both indices are sensitive to stiffness reduction. However, additional small fluctuations around the damage location were observed along the span, indicating sensitivity to multiple damage and localized capability.



(a) MCDI-Mode 1 (b) MSEDI-Mode 3 (c) MFDI-single damage

(d) MCDI-Mode 1 (e) MSEDI-Mode 3 (f) MFDI-multiple damage

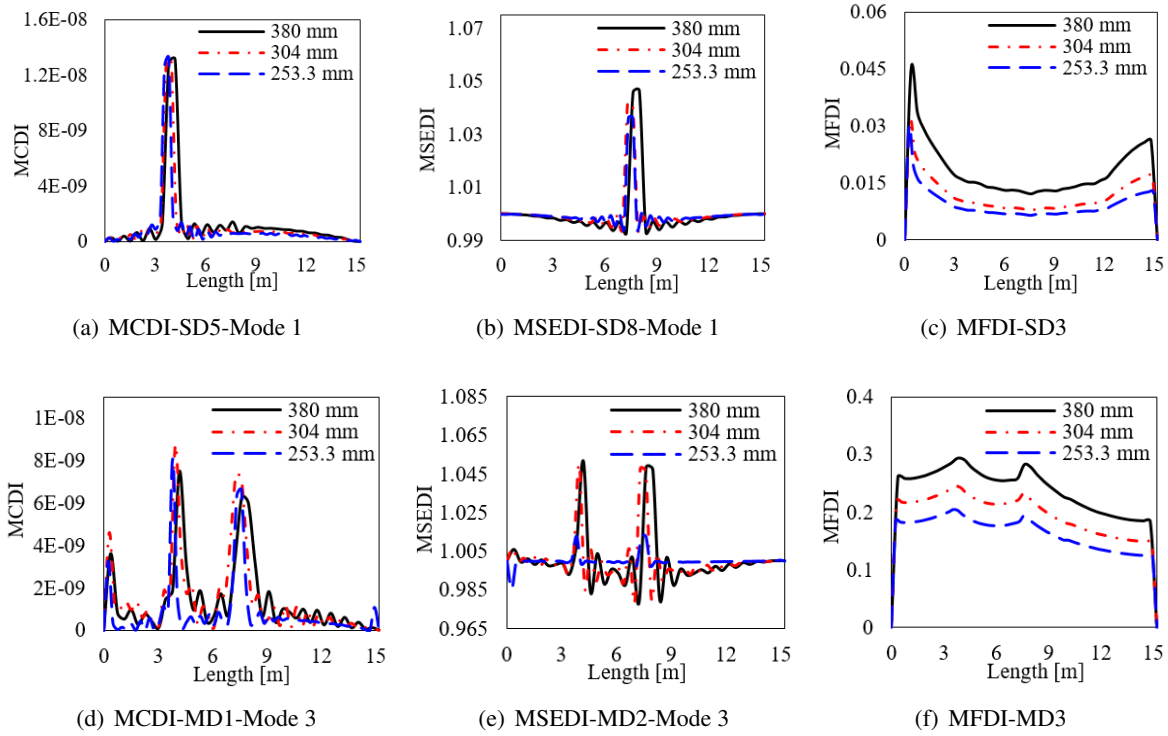
Figure 12. Visualization of MCDI, MSEDI, and MFDI

Figs. 12(c) and 12(f) demonstrate MFDI results for both single and multiple damage cases. Compared with MCDI and MSEDI, MFDI produced noticeable peaks at the damage locations even when all modes are included to determine the damage index. The peak MFDI values at damaged sections are higher than those in undamaged regions, while the background values remain low throughout the girder. In multiple damage cases, multiple peaks of similar index value are observed at each damage location, confirming the applicability of MFDI to identify cumulative damage effects. The peak positions match well with the actual damage locations, confirming accurate localization. Furthermore, the peak values increase with increasing damage severity (25% to 75% stiffness reduction), demon-

strating sensitivity to stiffness changes. Compared to MCDI and MSEDI, MFDI produced smoother curves with only one fluctuation near the boundary condition, indicating better robustness to multiple damage and localized capability. In this study, multiple damage cases were separated by approximately 3.8 m, and all indices produced distinct peaks at each damage location. For closely spaced damage, Fan and Qiao [17] showed that MCDI could still localize two damage sites separated by only 0.20 m, while Sokhangou et al. [29] found that very closely spaced cracks (5 cm) could only be identified as a single damage zone. The effect of closely spaced damage is recommended for future research.

4.3. Influence of mesh size

This section addresses the mesh size effect (380 mm, 304 mm, and 253.3 mm) on the damage identification results of the solid element model. The results indicated that mesh refinement primarily influences the quantification of damage indices, while the location of damage peaks remains stable across mesh sizes.



(a) MCDI-SD5-Mode 1 (b) MSEDI-SD8-Mode 1 (c) MFDI-SD3

(d) MCDI-MD1-Mode 3 (e) MSEDI-MD2-Mode 3 (f) MFDI-MD3

Figure 13. Visualization of mesh size comparison

For MCDI, Figs. 13(a) and 13(d) show the peak values corresponding to damage locations remain aligned with the actual damage position for all mesh sizes, confirming reliable localization. However, for the multiple damage case, the index value of the MCDI peak increases for a 304 mm mesh size. Moreover, the finest mesh (253.3 mm) produced unexpected peaks near the girder ends. This edge effect demonstrated that a finer mesh could increase fluctuation peaks in curvature-based calculations. A similar trend was observed for MSEDI, as shown in Figs. 13(b) and 13(e). Although all mesh sizes successfully identified the damage locations, the highest peak values were observed for the coarsest mesh (380 mm), followed by the 304 mm and 253.3 mm meshes, for the single damage case. The finest mesh (253.3 mm) indicated a trough value at the support region for the multiple damage case.

As shown in Figs. 13(c) and 13(f), MFDI produced peaks corresponding to the proposed damage locations for all mesh sizes, indicating effective damage localization for both the single and multiple damage cases. The MFDI peak values decreased with mesh refinement, with the highest peak values observed for the coarsest mesh (380 mm), followed by the 304 mm and 253.3 mm meshes. Despite this variation in peak magnitude, the overall MFDI distributions remained smooth, even for the finest mesh. This behavior indicated that MFDI is robust against mesh-induced fluctuation peaks and that mesh size primarily influences damage quantification rather than localization.

To quantify the effect of mesh size on localization accuracy, the localization error was evaluated for the single-damage case using MFDI. Following the localization approach adopted by Huang et al. [30], the detected damage location is defined as the position of the maximum damage-index peak. Table 3 shows that the MFDI localization error decreased from 2.50% for the 380 mm mesh to 2.00% and 1.67% for the 304 mm and 253.3 mm meshes, respectively. The detected peak was located at the first interior node adjacent to the support damage, indicating that localization accuracy improved as the mesh size decreased.

Table 3. Localization error for different mesh sizes

Damage index	Damage case	Mesh size (mm)	Actual damage location (m) (1)	Detected peak location (m) (2)	Localization error (%) (3)
MFDI	SD3	380 mm	0.000	0.380	2.50
MFDI	SD3	304 mm	0.000	0.304	2.00
MFDI	SD3	253.3 mm	0.000	0.253	1.67

Note: Localization error, (3) = |(2) – (1)| / L × 100%, L = 15.2 m.

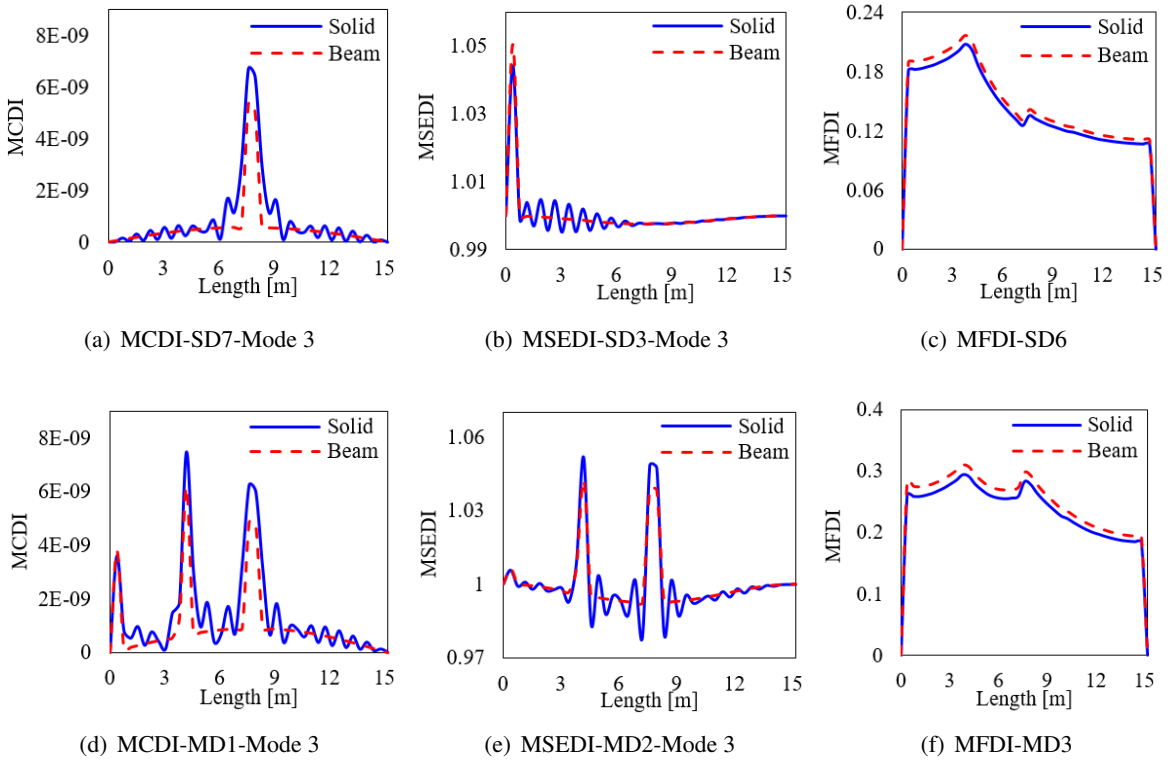
4.4. Comparison of solid and beam element models

In this section, the performance of the solid and beam element models is compared for MCDI, MSEDI, and MFDI under the SD1, SD4, and MD3 damage scenarios with a 380 mm mesh. For all three damage indices, the locations of the peaks obtained from both modeling approaches correspond to the predefined damage positions, indicating that, for the scenarios and mesh size considered here, element type has little effect on the accuracy of damage localization.

As depicted in Figs. 14(a) and 14(d), both solid and beam models demonstrated distinct peaks at the damaged sections, with Mode 3 considered for MCDI. The solid element model produced a higher peak index, showing additional local fluctuations along the undamaged regions. In contrast, the beam element model provided lower peak values with a smoother MCDI distribution. Despite these differences in index value, both models clearly localized the damaged regions and produced the same peak value at the support for multiple damage case. For MSEDI, Mode 3 provided effective damage localization in both solid and beam element models, as shown in Figs. 14(b) and 14(e). The beam model generated a higher peak index with a smoother MSEDI distribution similar to MCDI for the single damage case. However, the solid element model produced additional local fluctuations along the undamaged regions and higher peak indices at 1/4-span and 1/2-span for multiple damage case.

Both the solid and beam models identified the damaged sections in both the single and multiple damage cases when all mode shapes and natural frequencies were considered for MFDI. This status can be clearly seen in Figs. 14(c) and 14(f). The beam element model produced a high peak value of MFDI, while the solid element model provided a lower peak value. Despite these differences in

index value, both models clearly localized the damaged regions through the maximum index value along the girder. MFDI is less sensitive to local fluctuations within the undamaged regions, and the modeling approach primarily influences damage quantification more than localization.



(a) MCDI-SD7-Mode 3 (b) MSEDI-SD3-Mode 3 (c) MFDI-SD6

(d) MCDI-MD1-Mode 3 (e) MSEDI-MD2-Mode 3 (f) MFDI-MD3

Figure 14. Visualization of element type comparison

The localization accuracy of the solid and beam element models for the single-damage case was quantified and is summarized in Table 4. As shown in the table, both models detected the actual damage location at 3.800 m, providing a localization error of 0%. This result indicated that element type did not affect the MFDI localization accuracy for the single-damage case.

Table 4. Localization error for solid and beam element models

Damage index	Damage case	Element type	Actual damage location (m) (1)	Detected peak location (m) (2)	Localization error (%) (3)
MFDI	SD6	Solid	3.800	3.800	0.00
MFDI	SD6	Beam	3.800	3.800	0.00

Note: Localization error, (3) = |(2) – (1)| / L × 100%, L = 15.2 m.

5. Conclusions

This case study investigated the vibration-based damage identification of a W30×116 steel girder with a 15.2 m span using both beam and solid element models. Damage was simulated by reducing Young's modulus at three locations: support, 1/4-span, and 1/2-span with stiffness reductions of 25%, 50%, and 75%. The performance of three modal-based damage indices, namely the Modal Curvature

Damage Index (MCDI), Modal Strain Energy Damage Index (MSEDI), and Modal Flexibility Damage Index (MFDI), was evaluated under varying mesh sizes and modeling strategies. The following conclusions can be drawn as follows.

- Damage at 1/2-span resulted in more significant frequency shifts compared to damage at the support and at 1/4-span. The multiple damage cases provided a larger drop in frequency, indicating cumulative stiffness loss.

- Among the six mode shapes, Modes 1 and 3 consistently provided reliable damage localization across MCDI and MSEDI approaches, while higher modes were less sensitive due to their multiple curvature effects.

- MFDI was found to be highly effective in localizing damage for both single and multiple damage scenarios. In contrast to MCDI and MSEDI, which rely on individual mode shapes, MFDI integrates both natural frequency and mode shape data, combining contributions from multiple modes simultaneously.

- Mesh size was found to affect damage quantification more than damage localization. In the solid model for multiple damage cases with MCDI and MSEDI, higher mesh densities produced additional local index fluctuations at the girder edges. Similarly, the choice between solid and beam elements influenced the precision of damage quantification but had little effect on localization within the cases examined.

Furthermore, it should be noted that the reduction in Young's modulus used in this study represents an equivalent local stiffness loss rather than the actual geometry of corrosion or cracking. Therefore, validation using more realistic corrosion or crack models is recommended in future studies.

Declaration of generative AI and AI-assisted technologies

The author(s) declare that no generative AI or AI-assisted technologies were used in the preparation of this manuscript.

References

[1] Sun, Z., Santos, J., Caetano, E. (2022). Data-driven prediction and interpretation of fatigue damage in a road-rail suspension bridge considering multiple loads. *Structural Control and Health Monitoring*, 29(9): e2997.

[2] Deng, L., Wang, W., Yu, Y. (2016). State-of-the-art review on the causes and mechanisms of bridge collapse. *Journal of Performance of Constructed Facilities*, 30(2):04015005.

[3] Simoncelli, M., Aloisio, A., Zucca, M., Venturi, G., Alaggio, R. (2023). Intensity and location of corrosion on the reliability of a steel bridge. *Journal of Constructional Steel Research*, 206:107937.

[4] Zhang, G., Liu, Y., Liu, J., Lan, S., Yang, J. (2022). Causes and statistical characteristics of bridge failures: A review. *Journal of traffic and transportation engineering (English edition)*, 9(3):388–406.

[5] Aktan, A. E., Catbas, F. N., Grimmelsman, K. A., Tsikos, C. J. (2000). Issues in infrastructure health monitoring for management. *Journal of Engineering Mechanics*, 126(7):711–724.

[6] Chan, T. H. T., Thambiratnam, D. P., editors (2011). *Structural Health Monitoring in Australia*. Nova Science Publisher, New York Inc.

[7] Farrar, C. R., Worden, K. (2006). An introduction to structural health monitoring. *Philosophical Transactions of the Royal Society A: Mathematical, Physical and Engineering Sciences*, 365(1851):303–315.

[8] Worden, K., Dulieu-Barton, J. M. (2004). An overview of intelligent fault detection in systems and structures. *Structural Health Monitoring*, 3(1):85–98.

[9] Farrar, C. R., Worden, K. (2012). *Structural health monitoring: a machine learning perspective*. John Wiley & Sons.

[10] Barthorpe, R. J. (2010). On model-and data-based approaches to structural health monitoring. PhD thesis, University of Sheffield.

[11] Svendsen, B. T. (2021). *Numerical and experimental studies for damage detection and structural health monitoring of steel bridges*.

[12] Farrar, C. R., Doebling, S. W. (1997). An overview of modal-based damage identification methods. In *Proceedings of DAMAS conference*. Paper presented at the.

[13] Rytter, A. (1993). Vibrational Based Inspection of Civil Engineering Structures. PhD thesis, Dept. of Building Technology and Structural Engineering, Aalborg University. Fracture and Dynamics Vol. R9314 No. 44.

[14] Nick, H., Aziminejad, A. (2021). Vibration-based damage identification in steel girder bridges using artificial neural network under noisy conditions. *Journal of Nondestructive Evaluation*, 40(1):15.

[15] Nguyen, K.-D., Chan, T. H., Thambiratnam, D. P. (2016). Structural damage identification based on change in geometric modal strain energy–eigenvalue ratio. *Smart Materials and Structures*, 25(7):075032.

[16] Le, N. T., Thambiratnam, D., Nguyen, A., Chan, T. H. (2019). A new method for locating and quantifying damage in beams from static deflection changes. *Engineering Structures*, 180:779–792.

[17] Fan, W., Qiao, P. (2010). Vibration-based damage identification methods: A review and comparative study. *Structural Health Monitoring*, 10(1):83–111.

[18] Rucevskis, S., Janeliukstis, R., Akishin, P., Chate, A. (2016). Mode shape-based damage detection in plate structure without baseline data. *Structural Control and Health Monitoring*, 23(9):1180–1193.

[19] Granhaug, E. B., Pontseele, L. A. G. V. D. (2018). Modal Analysis and Damage Identification of the Hell Bridge Test Arena. Master's thesis, NTNU.

[20] Pandey, A. K., Biswas, M., Samman, M. M. (1991). Damage detection from changes in curvature mode shapes. *Journal of sound and vibration*, 145(2):321–332.

[21] Stubbs, N., Kim, J., Topole, K. (1992). An efficient and robust algorithm for damage localization in offshore platforms. In *Proceedings of ASCE 10th Structures Congress*, New York, USA, 543–546.

[22] Stubbs, N., Kim, J.-T., Farrar, C. (1995). Field verification of a nondestructive damage localization and severity estimation algorithm. In *Proceedings-SPIE the international society for optical engineering*. Paper presented at the.

[23] Stubbs, N., Kim, J.-T. (1996). Damage localization in structures without baseline modal parameters. *AIAA Journal*, 34(8):1644–1649.

[24] Kim, J.-T., Stubbs, N. (2002). Improved damage identification method based on modal information. *Journal of sound and vibration*, 252(2):223–238.

[25] Pandey, A. K., Biswas, M. (1994). Damage detection in structures using changes in flexibility. *Journal of sound and vibration*, 169(1):3–17.

[26] Wahalathantri, B. L., Thambiratnam, D., Chan, T. H., Fawzia, S. (2009). Assessment of "change in flexibility method" in structural health monitoring systems. In *Proceedings of the 3rd Smart Systems Postgraduate Student Conference*. Paper presented at the.

[27] Farrar, C. R., Cornwell, P. J., Doebling, S. W., Prime, M. B. (2000). *Structural health monitoring studies of the Alamosa Canyon and I-40 bridges*. No. LA-13635-MS, Los Alamos National Lab. (LANL), Los Alamos, NM (United States).

[28] Le, N. T. (2019). Structural damage identification using static and modal flexibility-based deflections. PhD thesis, Queensland University of Technology. Queensland University of Technology.

[29] Sokhangou, F., Sorelli, L., Chouinard, L., Dey, P., Conciatori, D. (2024). Detecting multiple damages in UHPFRC beams through modal curvature analysis. *Sensors*, 24(3):971.

[30] Huang, Z., Chu, X., Liu, X., He, Q., Zhou, Z. (2026). Structural damage localization via RPCA-based decomposition of full-field responses with a differential damage index. *Applied Sciences*, 16(13):6504.